AIP Advances

Nano-indentation mechanical characterizations of solution processed inorganic metal oxide thin films and influence of grain size

Cite as: AIP Advances **10**, 105016 (2020); https://doi.org/10.1063/5.0020213
Submitted: 01 July 2020 . Accepted: 18 September 2020 . Published Online: 09 October 2020

Sana Ullah, Fabio De Matteis, Massimiliano Lucci, and Ivan Davoli

Nano-indentation mechanical characterizations of solution processed inorganic metal oxide thin films and influence of grain size

Cite as: AIP Advances 10, 105016 (2020); doi: 10.1063/5.0020213
Submitted: 1 July 2020 • Accepted: 18 September 2020 •
Published Online: 9 October 2020

Sana Ullah,[1,a] Fabio De Matteis,[2] Massimiliano Lucci,[3] and Ivan Davoli[3]

AFFILIATIONS

[1] Department of Mechanical Engineering, Khwaja Fareed University of Engineering and Information Technology, Abu Dhabi Road, 64200 Rahim Yar Khan, Pakistan
[2] Dipartimento di Ingegneria Industriale, Università Degli Studi di Roma "Tor Vergata", Via del Politecnico, 1, 00133 Roma, Italy
[3] Dipartimento di Fisica, Università degli Studi di Roma "Tor Vergata", Via della Ricerca Scientifica, 1, 00133 Roma, Italy

[a] **Author to whom correspondence should be addressed:** sanaullahzafar@yahoo.com and sana.ullah@kfueit.edu.pk

ABSTRACT

Aluminum-doped zinc oxide thin films were prepared by solution synthesis where molarity concentrations and mixing ratios for oxide and dopant sources were changed while deposition and pre- and post-deposition annealing steps remained the same. Post-deposition high-temperature annealing is known to improve conductivity and transparency but may deteriorate the mechanical characteristics of films. However, we report the successful preparation of thin films with high mechanical hardness (>11 MPa) and reduced modulus (>10^2 MPa) along with high electro-optical characteristics even after multiple annealing steps. Changes in grain sizes because of changes in molarity concentrations and difference of atomic radii caused mechanical characteristics of films. Both regular and inverse Hall–Petch relations were observed.

I. INTRODUCTION

Transparent conducting films (TCFs) are used in diverse applications from portable devices to open-air photovoltaic solar cell systems. In addition to transparency and conductivity, successful TCFs have robust mechanical properties of hardness, toughness, and adhesion throughout their lifetime. Grain size is considered the single most relevant element imparting mechanical strength and hardness to thin films. According to Hall–Petch, hardness increases with a decrease in grain size.[1] However, an inverse relation between film strength and grain size has also been observed.[2] Hence, there should be a critical grain size at which point a favorable microstructure imparts maximum strength and/or hardness and at which the Hall–Petch relation is exactly followed. In multi-component carbide films in which mixed elements are deposited by non-reactive DC magnetron sputtering, the microstructure is the most important factor for high hardness.[3] Similarly, in thin films prepared by reactive DC magnetron sputtering,[4] chemical vapor deposition,[5] and RF magnetron sputtering,[6] hardness is mostly affected by microstructural (grain size, orientation, texture, and so forth) changes. Grain size has also been reported to affect electrical conductivity,[7,8] Young's modulus,[9,10] and yield stress[11] of metals.

In this study, we created aluminum-doped zinc oxide (AZO) TCFs through solution synthesis. We characterized these TCFs' mechanical properties by the nano-indentation technique and determined the role of grain size. Grain size proved to play a pivotal role in determining the mechanical properties of the deposited films. In addition, changing the molarity concentrations and precursor mixing ratios resulted changes in grain size that, in turn, directly impacted hardness and the reduced modulus. We successfully obtained TCFs with acceptable electrical conductivity and optical transparency in addition to robust mechanical characteristics.[12]

II. MATERIALS AND METHODS

First, we obtained AZO TCFs through spin coating deposition and then characterized these TCFs for hardness and the reduced

modulus. Oxide and dopant source solutions were prepared separately and mixed in different volume proportions to get precursor solutions. The oxide source was prepared by solution combustion synthesis (SCS), while the dopant source was prepared by simple solution synthesis (SSS).

SCS is a process in which exothermic redox reactions deliver the energy needed to form metal oxides. The process was first reported in a previous study[13] wherein fine particle oxides were obtained. The ingredients for SCS consist of a metal-oxidizing source (usually a metal nitrate) and a "fuel" as the reducing agent (typically urea). On the other hand, SSS does not use a fuel. Since SCS was first reported, the process has gained tremendous popularity and has been widely employed for the preparation of oxides and a large variety of nanomaterials.[14]

SCS was used to prepare metal oxide source solution wherein zinc nitrate hexahydrate [$Zn(NO_3)_2{\cdot}6H_2O$, Sigma Aldrich, 98%, CAS Number 10196-18-6] as a metal-oxidizing source was dissolved in 2-methoxyethanol (2-MEA, $C_3H_8O_2$, Fluka, 99%, CAS Number 109-86-4) solvent; urea [$CO(NH_2)_2$, Sigma Aldrich, 98%, CAS Number 57-13-6] was added as a fuel while the oxide source and fuel were kept at 1:1 molar proportion. All reagents were used as purchased. SSS was used to prepare the dopant source solution wherein aluminum chloride hydrate ($AlCl_3{\cdot}6H_2O$, Sigma Aldrich, 99%, CAS Number: 7784-13-6) was dissolved in 2-MEA solvent without any fuel component. Each of the source solutions was prepared separately at molarities (M) of 0.5 M, 0.25 M, and 0.1 M. Then, each was mixed at two volume proportions (9:1 and 8:2). The three different molarities and two mixing ratios resulted in six distinct precursor solutions for deposition of thin films. Each solution was stirred at 60 °C for 2 h to dissolve all ingredients until clear and homogeneous solutions were obtained. Then, the solutions were aged for 2 days at room temperature. After this, but before deposition of thin films, the solutions were homogenized by stirring again at 60 °C for 10 min and cooled to room temperature. Corning glass substrates were cleaned in an ultrasonic bath at 60 °C for 15 min in acetone and for 15 min in 2-isopropanol and dried with N_2. Then, they were cleaned and dried through a 30 min UV/ozone surface activation step using the PSD-UV Novascan system. Thin films were sequentially produced by spin coating each precursor solution onto the glass substrates for 30 s at 3000 rpm. When a layer was deposited, the substrate was kept on the heating plate at 400 °C for 10 min in ambient to evaporate solvent and any residuals. A stack of ten films were created following the same procedure. The stacks were placed in an oven at room temperature for 1 h and exposed to 10 °C/min increase in temperature until reaching 600 °C. Then, the stacks were removed and cooled to room temperature. Next, each stack was subjected to rapid thermal annealing (RTA), first in a vacuum at 500 °C and then in N_2–5%H_2 at 600 °C, for 10 min each.

TABLE I. Operating parameters for nano-indentation measurements.

Maximum load	5 mN
Time of maximum fixed load	10 s
Indentation depth	120 nm
Penetration speed/load control	2 mN/s
Matrix	6 × 6
Type of indenter probe	Diamond Berkovitch

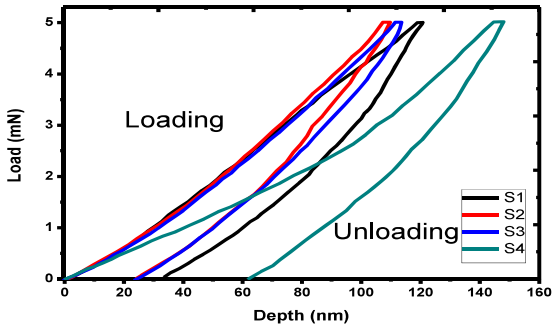

FIG. 1. Applied load vs penetration depth.

To determine the structure of the films, x-ray diffraction (XRD) analysis was done using the Panalytical X'Pert PRO diffractometer in Bragg–Brentano ($\theta/2\theta$ coupled) geometry with Cu Kα line radiation (λ = 1.540 598 A) in the 2θ range from 10° to 80°. A Perkin Elmer Lambda 950 UV/VIS/NIR spectrometer was used to observe the transparency of the films by measuring the total optical transmission in the range of 200 nm–2500 nm. The details of structural, electrical, optical, and surface analysis of these thin films are reported in Ref. 12.

Hardness and the reduced modulus were determined by using Nano Test Vantage by Micro Materials Ltd. The operating parameters are given in Table I. The indentation depth was well within the desired limit to avoid substrate effects on the measurements. The applied load was deliberately kept low to avoid the influence of the substrate. In this way, the measured values reflected the true mechanical characteristics of the obtained thin films. Full-width at half maximum (FWHM) was employed to determine the average grain size using the Debye–Scherer formula $D = k\lambda/B\cos\theta$ applied to the XRD results, where λ is the x-ray wavelength (1.540 598 Å), θ is the Bragg angle, k is a constant with a value of 0.9, and **B** is FWHM.

The thicknesses of the layer stacks vary due to the differences in the molarities of the precursors. However, no direct effect of film thickness and substrate on the measured values was observed. This was further confirmed by the smooth loading and unloading responses of samples against the applied load, as shown in Fig. 1.

III. RESULTS AND DISCUSSIONS

Our aim was to develop TCFs with robust mechanical strengths. Only molarity and volume mixing ratios were varied while spin-coating; the number of layers in each film stack and pre- and post-deposition annealing was kept equal for all films. This helped us to analyze the pivotal role of grain size in determining the mechanical and electro-optical properties of the prepared AZO TCFs.

We used XRD analyses to determine the physical structure and crystallinity behavior of the films. The diffraction curves are given in Fig. 2.

The thin films showed strong c-axis orientation with a hexagonal wurtzite crystal structure typical of ZnO. The prominent peak at 34° with (002) orientation and other peaks at 31° and 36° with

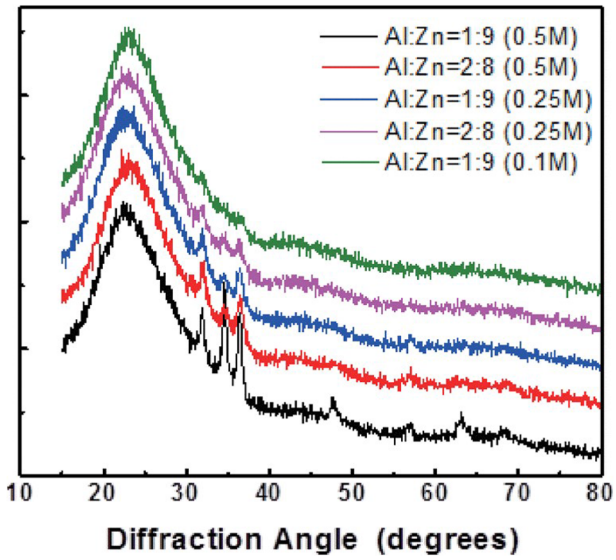

FIG. 2. XRD curves obtained for thin films. Reprinted with permission from Ullah *et al.*, in 15th IEEE International Conference on Nanotechnology (IEEE, Rome, Italy, 2015), pp. 144–147.

(010) and (011) diffraction orientations, respectively, are characteristic ZnO peaks and indicate the polycrystalline structure of the films. These peaks decreased in intensity with the decreasing concentration of the ZnO source material in the precursor solutions. This trend is also shown within the same molarity concentration wherein the intensity of curves decreased as the oxide source solution concentration decreased. The appearance of these typical peaks with variation in intensity as per changing molarity concentrations is ascribed to self-texturing phenomena.[15]

Optical transparency is another important property of TCFs, and our results are given in Fig. 3.

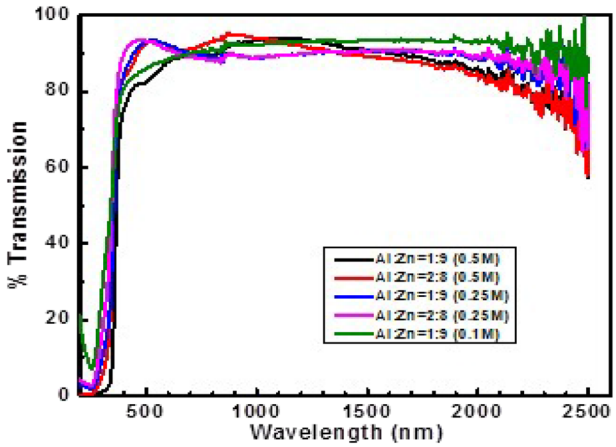

FIG. 3. Optical transmission response of thin films. Reprinted with permission from Ullah *et al.*, in 15th IEEE International Conference on Nanotechnology (IEEE, Rome, Italy, 2015), pp. 144–147.

All of our thin films showed more than 80% transmission in the visible light and higher wavelengths, from 400 nm to 1200 nm. This is noted that for one molarity, optical transparency is high for the precursor solution in which the amount of the oxide source material is low.

Here, we report mechanical nano-indentation characterizations for hardness and the reduced modulus. Table II lists the molar concentrations and precursor mixing ratios for each sample. As samples **S5** and **S6** had high electrical resistances due to the lower molar concentrations of oxide and dopant sources, these were not characterized.

The grain size data are given in Table III.

Grains were bigger in films prepared from solutions of higher molarity (**S1** vs **S3** and **S2** vs **S4**). For thin films fabricated from solutions of the same molarity, grains were larger at higher mixing ratios of oxide source solution (compare **S1** with **S2** and **S3** with **S4**). On the flip side, the grain size decreased with a decrease in the oxide source solution ratio in a precursor. The hardness and reduced modulus values for the AZO thin films are reported in Table IV.

Our films showed both a direct and an inverse Hall–Petch relation. This is also evident from the results reported in Table IV that indicate that the grain size decreased as the molarity decreased. Within a given molarity, the grain size decreased with a decrease in the mixing ratio of the oxide source. However, at a high molarity, a direct Hall–Petch relation was followed where the decreasing grain size increased both hardness and the reduced modulus. As detailed in Table IV and in Fig. 4, at a higher molarity of 0.5M, the grain size decreased as the oxide source ratio decreased and the dopant source ratio increased in precursor solutions. The same was true for 0.25M films. For 0.5M films, hardness and the reduced modulus increased as the grain size decreased, following a direct Hall–Petch relation. In the case of films from 0.25M solutions, hardness and the reduced modulus decreased with the decreasing grain size. As shown in Fig. 4, both hardness and the reduced modulus decreased with the decreasing molarity as per the Hall–Petch relation.[1]

We also found that hardness first increased, remained the same over a range of grain sizes, and then decreased with further increases in grain size, following a typical Hall–Petch relation. Figure 5 shows the hardness and reduced modulus values for thin film samples against the applied load.

The data further indicate that, at a critical grain size, films have the maximum hardness and reduced modulus. Both of these mechanical characteristics deteriorate as the grain size increases or decreases beyond this critical value. As the samples increase or

TABLE II. Molar concentrations and volume mixing ratios for different samples.

Sample ID	Molarity (M)	Precursor ratio (in volume) (oxide source: dpant source)
S1	0.5	9:1
S2	0.5	8:2
S3	0.25	9:1
S4	0.25	8:2
S5	0.1	9:1
S6	0.1	8:2

TABLE III. Grain size values calculated for samples using the Scherer formula.

Sample ID	Peak	Grain size (Å)	Average grain size	Sample ID	Peak	Grain size (Å)	Average grain size
	31.89	140 ± 8			31.91	121 ± 15	
S1	34.60	187 ± 6	168 ± 7	**S3**	34.61	224 ± 115	138 ± 35 (163 ± 49)
	36.43	171 ± 6			36.43	145 ± 18	
	31.99	126 ± 14			31.90	100 ± 23	
S2	34.75	108 ± 29	113 ± 18	**S4**	34.68	102 ± 34	78 ± 19 (88 ± 22)
	36.51	105 ± 10			36.51	62 ± 10	

TABLE IV. Hardness and reduced modulus data of thin films.

Sample ID	Molarity/mixing ratio (Zn:Al)	Maximum load (mN)	Plastic depth (nm)	Average hardness (GPa)	Average reduced modulus (GPa)
S1	0.5/9:1	5.216 ± 0.009	83.34 ± 13.32	15.756 59 ± 3.514	136.097 56 ± 18.411
S2	0.5/8:2	5.218 ± 0.010	71.39 ± 12.87	19.804 70 ± 4.608	147.965 06 ± 17.412
S3	0.25/9:1	5.217 ± 0.009	71.75 ± 11.98	19.530 24 ± 4.175	137.005 62 ± 13.745
S4	0.25/8:2	5.217 ± 0.010	102.64 ± 16.85	11.671 36 ± 3.008	102.026 07 ± 13.421

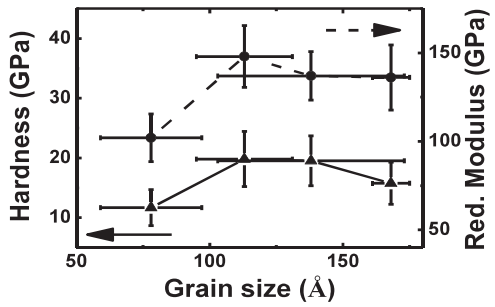

FIG. 4. Grain size vs hardness and reduced modulus.

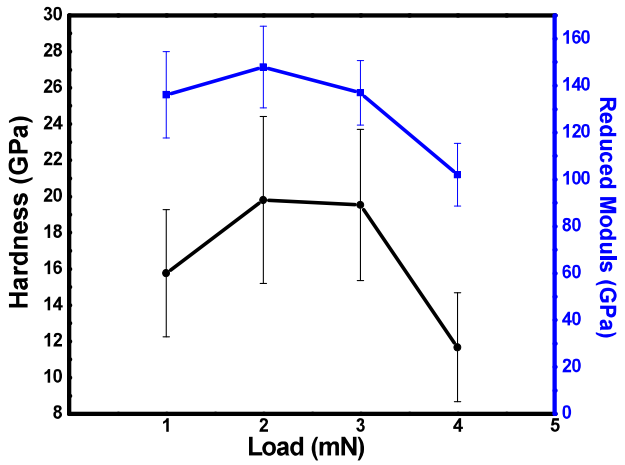

FIG. 5. Hardness and reduced modulus for samples at different applied loads.

decrease in grain size, their mechanical strength decreases across the critical value.

Grain size is important in terms of electrical resistivity of thin films as well. As the grain size decreases, the number of grains increases that increases grain boundaries and surfaces. The increase in the number of grains, therefore, increases grain-boundary and surface scattering, which, in turn, increases the electrical resistivity of thin films. Figure 6 shows the influence of grain size on the electrical sheet resistance of thin films. We observe that the electrical resistivity of thin films decreased with the increasing grain size. The results are in line with the observations made for nano-crystalline

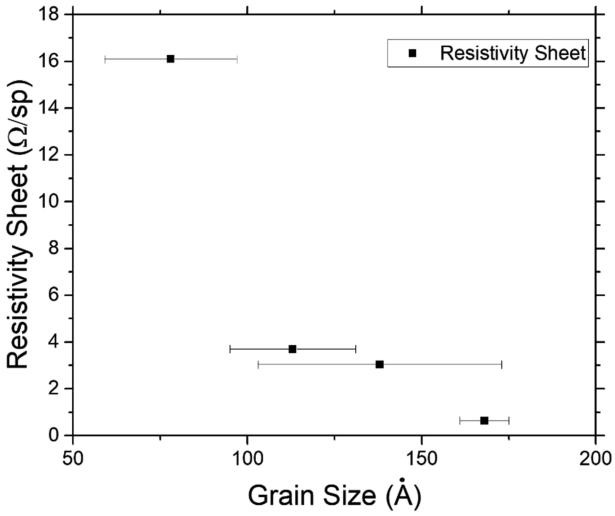

FIG. 6. Sheet resistivity response in terms of grain size.

TABLE V. Experimental and nano-indentation measurement results.

Sample ID	S1	S2	S3	S4
Molarity (M)	0.5	0.5	0.25	0.25
Mixing ratio	Zn:Al = 9:1	Zn:Al = 8:2	Zn:Al = 9:1	Zn:Al = 8:2
Resistivity (sheet) $\times 10^3$ ($\Omega/\square$)	0.64	3.70	3.04	16.1
Resistivity (bulk) (Ω cm)	0.032	0.185	0.152	0.805
Mobility (cm^2/V s)	9.21	26.1	2.31	4.4
Concentration $\times 10^{18}$ (cm^{-3})	21.15	1.291	11.78	0.014
Grain size (Å)	168	113	138	78
Hardness (GPa)	15.76	19.8	19.53	11.67
Modulus (GPa)	136.09	147.96	137.01	102.03

ZnO wherein the grain size affected the electrical conductivity of doped and un-doped ZnO.[16]

Overall, our results show that AZO TCFs can be produced through solution synthesis, avoiding vacuum deposition. Our films had high mechanical hardness and reduced modulus even though they were subjected to multiple post-deposition annealing treatments. Changing molarity and mixing ratios of oxide and dopant source materials can render thin films with better electro-optical properties. Such alternative thin films are also mechanically stable with high hardness and reduced modulus and are suitable for their applications in adverse environments.

The mechanical strength of a material can be improved in many ways, such as through strain hardening, solid solution strengthening, and so forth. Another way is to limit the motion of crystalline imperfections known as dislocations. Grain size plays an important role in this effort as dislocations travel through grains. Once a dislocation reaches a grain boundary, it stops unless enough stress or thermal energy is provided for further movement. A decrease in grain size translates into more grain boundaries, which increases the chances that a dislocation will be stopped (by one of the many grain boundaries). This increases the strength of the material and explains how the grain size is a main parameter determining hardness and the reduced modulus. However, there is a critical grain size at which the maximum hardness and reduced modulus are achieved. Both decrease as the grain size decreases below or increases above this critical size.[1] Our results showed this pattern. The grain size decreased as the molarity decreased. In line with this behavior, hardness and the reduced modulus continuously decreased. This decrease in modulus was also observed in a previous study[17] wherein the elastic modulus continuously decreased with the decreasing grain size.

As the annealing procedure was the same for all films, we observed that the grain growth was hindered by the Al content. As the Al dopant source increased, the grain size decreased. This was true for molar concentrations of oxide and dopant sources and across their mixing ratios and has previously been reported.[18] With the decreasing grain size, the mechanical characteristics improved (samples S1 and S2), and films showed a direct Hall–Petch relation. On the other hand, as the grain size goes below the critical grain size, both hardness and the reduced modulus decrease (samples S3 and S4), showing the inverse Hall–Petch relation. Our results are in line with the previous reports.[19–21] Molar concentrations, oxide and dopant sources mixing ratios, respective grain sizes, hardness, and reduced modulus for all the samples are listed in Table V.

IV. CONCLUSIONS

We report the preparation of TCFs through solution synthesis that showed desirable electro-optical properties as well as robust mechanical strength. The grain size played a pivotal role in determining the mechanical characteristics and could be controlled by using different molar concentrations and mixing ratios of ingredients in precursor solutions.

ACKNOWLEDGMENTS

F.D.M. acknowledges research Project No. 85-2017-15173 of the Lazio region according to L.R. 13-08 (Progetto NARAS).

The authors do not have any conflicts of interest to report.

DATA AVAILABILITY

The data that support the findings of this study are available within the article.

REFERENCES

[1] T. G. Nieh and J. Wadsworth, "Hall–Petch relation in nanocrystalline solids," Scr. Metall. Mater. **25**, 955–958 (1991).

[2] S. Ullah, M. Lucci, F. De Matteis, and I. Davoli, "Mechanical characterization of stacked thin films: The cases of aluminum zinc oxide and indium zinc oxide grown by solution and combustion synthesis," Thin Solid Films **640**, 109–115 (2017).

[3] P. Malinovskis, S. Fritze, L. Riekehr, L. von Fieandt, J. Cedervall, D. Rehnlund, L. Nyholm, E. Lewin, and U. Jansson, "Synthesis and characterization of multicomponent (CrNbTaTiW)C films for increased hardness and corrosion resistance," Mater. Des. **149**, 51–62 (2018).

[4] S. Anwar, S. Anwar, and P. Nayak, "Multilayer composite ceramic-metal thin film: Structural and mechanical properties," Surf. Interfaces **10**, 110–116 (2018).

[5] L. von Fieandt, K. Johansson, T. Larsson, M. Boman, and E. Lindahl, "On the growth, orientation and hardness of chemical vapor deposited Ti(C,N)," Thin Solid Films **645**, 19–26 (2018).

[6] A. K. Battu, S. Manandhar, and C. V. Ramana, "Nanomechanical characterization of titanium incorporated gallium oxide nanocrystalline thin films," Mater. Today Nano. **2**, 7–14 (2018).

[7] T. Salkus, E. Kazakevicius, J. Banys, M. Kranjcec, A. A. Chomolyak, Y. Y. Neimet, and I. P. Studenyak, "Influence of grain size effect on electrical properties of Cu6PS5I superionic ceramics," Solid State Ionics **262**, 597–600 (2014).

[8] A. Kumar, D. Singh, and D. Kaur, "Grain size effect on structural, electrical and mechanical properties of NiTi thin films deposited by magnetron co-sputtering," Surf. Coat. Technol. **203**, 1596–1603 (2018).

[9]J. Lian, S.-W. Lee, L. Valdevit, M. I. Baskes, and J. R. Greer, "Emergence of film-thickness- and grain-size-dependent elastic properties in nanocrystalline thin films," Scr. Mater. **68**, 261–264 (2013).
[10]J. D. Giallonardo, U. Erb, K. T. Aust, and G. Palumbo, "The influence of grain size and texture on the Young's modulus of nanocrystalline nickel and nickel–iron alloys," Philos. Mag. **91**(36), 4594–4605 (2011).
[11]E. N. Borodin, A. E. Mayer, and P. N. Mayer, "Grain size dependence of the yield stress for metals at quasistatic and dynamic loadings," in *13th International Conference on Fracture* (Curran Associates, Inc., China, 2014), pp. 16–21.
[12]S. Ullah, F. De Matteis, R. Branquinho, E. Fortunato, R. Martins, and I. Davoli, "A combination of solution synthesis and solution combustion synthesis for highly conducting and transparent aluminum zinc oxide thin films," in *15th IEEE International Conference on Nanotechnology* (IEEE, Rome, Italy, 2015), pp. 144–147.
[13]K. C. Patil, S. T. Aruna, and S. Ekambaram, "Combustion synthesis," Curr. Opin. Solid State Mater. Sci. **2**, 158–165 (1997).
[14]S. T. Aruna and A. S. Mukasyan, "Combustion synthesis and nanomaterials," Curr. Opin. Solid State Mater. Sci. **12**, 44, 50 (2008).
[15]H. Deng, J. J. Russell, R. N. Lamb, B. Jiang, Y. Li, and X. Y. Zhou, "Microstructure control of ZnO thin films prepared by single source chemical vapor deposition," Thin Solid Films **458**, 43–46 (2004).
[16]C.-w. Nan, A. Tschöpe, S. Holten, H. kliem, and R. Birringer, "Grain-size dependent electrical properties of nanocrystalline ZnO," J. Appl. Phys. **85**, 7735–7740 (1999).
[17]R. Chaim and M. Hefetz, "Effect of grain size on elastic modulus and hardness of nanocrystalline ZrO_2-3 wt% Y_2O_3 ceramic," J. Mater. Sci. **39**, 3057–3061 (2004).
[18]R. Siddheswaran, R. V. Mangalaraja, R. E. Avila, D. Manikandan, C. Esther Jeyanthi, and S. Ananthakumar, "Evaluation of mechanical hardness and fracture toughness of Co and Al co-doped ZnO," Mater. Sci. Eng., A **558**, 456–461 (2012).
[19]C.-Y. Yen, S.-R. Jian, G.-J. Chen, C.-M. Lin, H.-Y. Lee, W.-C. Ke, Y.-Y. Liao, P.-F. Yang, C.-T. Wang, Y.-S. Lai, S.-C. Jang, and J.-Y. Juang, "Influence of annealing temperature on the structural, optical and mechanical properties of ALD-derived ZnO thin films," Appl. Surf. Sci. **257**, 7900–7905 (2011).
[20]Y. Cao, S. Allameh, D. Nankivil, S. Sethiaraj, T. Otiti, and W. Soboyejo, "Nanoindentation measurements of the mechanical properties of polycrystalline Au and Ag thin films on silicon substrates: Effects of grain size and film thickness," Mater. Sci. Eng., A **427**, 232–240 (2006).
[21]L. Chi-ming, L. Keh-moh, and R. Stella, "Effect of annealing temperature on the quality of Al-doped ZnO thin films prepared by sol–gel method," J. Sol-Gel Sci. Technol. **61**(1), 249–257 (2012).